THE JOURNAL OF NAVIGATION (2003), **56**, 475–486.
DOI: 10.1017/S0373463303002443 Printed in the United Kingdom

Effective Cycle Slip Detection and Identification for High Precision GPS/INS Integrated Systems

Hung-Kyu Lee, Jinling Wang and Chris Rizos

(*The University of New South Wales*, *Australia*)

To ensure high accuracy results from an integrated GPS/INS system, the carrier phase observables have to be used to update the filter's states. As a prerequisite the integer ambiguities must be resolved *before* using carrier phase measurements. However, a cycle slip that remains undetected (and uncorrected) will significantly degrade the filter's performance. In this paper, an algorithm that can effectively detect and identify any type of cycle slip is presented. The algorithm uses additional information provided by the INS, and applies a statistical technique known as the cumulative-sum (CUSUM) test. In this approach, cycle slip decision values can be computed from the INS-predicted position (due to the fact that its short-term accuracy is very high), and the CUSUM test used to detect cycle slips (as it is very sensitive to abrupt changes of mean values). Test results are presented to demonstrate the effectiveness of the proposed algorithm.

KEY WORDS

1. Cycle Slip. 2. CUSUM Test. 3. GPS/INS Integration.

1. INTRODUCTION. Integrated GPS/INS systems have been widely used in kinematic positioning and navigation for many years. Typical applications include vehicle navigation, guidance and control, as well as aerial photogrammetry, airborne gravity survey, mobile mapping. In such integrated systems, low data rate, high accuracy GPS measurements can be used to estimate and to correct the error states of the INS within a tightly coupled integration filter. In order to obtain high precision positioning results with such a system, GPS carrier phase observables are typically used in the filter update. However, it is usual for the integer ambiguities to be resolved before the measurements can be utilized in the update. These ambiguities remain constants as long as no loss of signal lock occurs. In the event of signal loss, the integer counter is reinitialised, effectively causing a jump in the instantaneous accumulated phase by an integer number of cycles. Such a jump (as indicated in Figure 1), is called a cycle slip, and corrupts the carrier phase measurement, causing the unknown ambiguity value to be different after the cycle slip compared with its value before the slip. It must be repaired before the phase data is processed as double-differenced observables (Rizos, 1999).

There are three causes of cycle slips (Hofmann-Wellenhof *et al.*, 2001). First, cycle slips are induced by obstructions of the satellite signal due to trees, building, and so

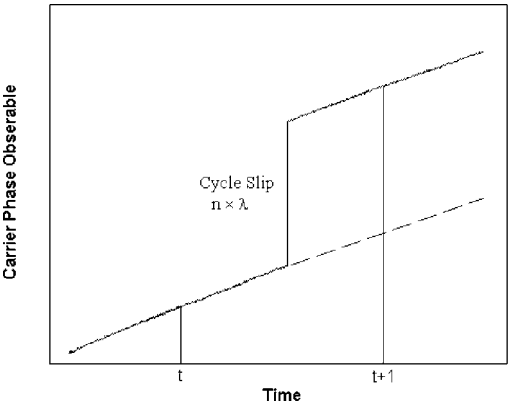

Figure 1. Cycle slip on GPS carrier phase observables.

on. The second cause is a low signal to noise ratio (SNR) due to extreme ionospheric conditions, multipath, high receiver dynamics, or low satellite elevation. The third cause is internal receiver tracking problems, reflected in incorrect signal processing. The occurrence of an undetected cycle slip will significantly degrade the accuracy of the navigational solution obtained from the integration system. Therefore a number of techniques for the detection and identification of cycle slips have been developed. Some examples, as in the case of standalone GPS, include the use of GPS Doppler frequency (Cannon, 1987), linear combinations of L1 and L2 observables such as the geometry-free combination (Blewitt, 1990; Dedes & Mallett, 1995) and widelane phase minus narrowlane pseudorange (Han, 1997; Gao & Li, 1999). On the other hand, integration of GPS with INS is appropriate for detection and identification of small cycle slips. In such a system the high relative accuracy of the INS output can be used to predict the GPS antenna position at the measurement, with periodic INS error update by GPS observables (Wei *et al*., 1992; Schwarz *et al*., 1994). In addition, such an approach can overcome the drawbacks of GPS standalone techniques that are not sensitive to dynamics, as it does not rely exclusively on GPS measurements (Gao, 1992; Altmayer, 2000).

In this paper a cycle slip detection and identification algorithm that can be easily implemented in an integrated GPS/INS system will be proposed. The algorithm uses the GPS antenna position provided by the INS to calculate cycle slip decision values, and applies the cumulative-sum (CUSUM) test to small persistent changes in the mean and/or standard deviation of measurements.

2. A CYCLE SLIP DETECTION & IDENTIFICATION ALGORITHM.

2.1. *Decision Value*. The basic task of the algorithm is to compare the double-differenced GPS carrier phase observables $\nabla\Delta\phi^{GPS}$ with the double-differenced geometric distances $\nabla\Delta\phi^{INS}$ computed using INS-predicted GPS antenna positions:

$$\delta\nabla\Delta\phi = \nabla\Delta\phi^{GPS} - \nabla\Delta\phi^{INS}. \tag{1}$$

https://doi.org/10.1017/S0373463303002443 Published online by Cambridge University Press

Denoting $\delta\nabla\Delta\phi$ to be the cycle slip decision values. In Equation (1), the GPS double-differenced measurement can be defined as follows:

$$\begin{aligned}\nabla\Delta\phi^{GPS} &= \phi_U^k - \phi_U^j - \phi_R^k + \phi_R^j \\ &= \frac{1}{\lambda}\nabla\Delta\rho_{UR}^{kj} + \nabla\Delta N_{UR}^{kj} - \nabla\Delta d_{ion} + \nabla\Delta d_{trop} + \nabla\Delta m + \nabla\Delta\varepsilon^{GPS},\end{aligned} \tag{2}$$

where, λ is the wavelength of GPS carrier phase measurement, $\nabla\Delta\rho_{UR}^{kj}$ is the double-differenced true geometric distances, $\nabla\Delta N_{UR}^{kj}$ is the double-differenced integer ambiguities, $\nabla\Delta d_{ion}$ is the ionospheric delay, $\nabla\Delta d_{trop}$ is the tropospheric delay, $\nabla\Delta m$ is multipath, and $\nabla\Delta\varepsilon$ is the remaining biases and measurement noise. The computation of the double-differenced geometric distances is based on the INS-predicted positions:

$$\begin{aligned}\nabla\Delta\phi^{INS} &= \frac{1}{\lambda}\left\{\rho_U^k - \rho_U^j - \rho_R^k + \rho_R^j\right\} \\ &= \frac{1}{\lambda}\nabla\Delta\rho_{UR}^{kj} + \nabla\Delta\varepsilon^{INS},\end{aligned} \tag{3}$$

where $\nabla\Delta\varepsilon^{INS}$ represents the error introduced by the INS-predicted GPS antenna positions and the satellite ephemeris error. Hence, decision value $\delta\nabla\Delta\phi$ can be expressed as follows:

$$\delta\nabla\Delta\phi = \nabla\Delta N_{UR}^{kj} - \nabla\Delta d_{ion} + \nabla\Delta d_{trop} + \nabla\Delta m + \nabla\Delta\varepsilon^{GPS} + \nabla\Delta\varepsilon^{INS}. \tag{4}$$

2.2. *Statistical Properties of the Decision Value.* There are a number of error sources that contaminate GPS carrier phase measurements, including satellite ephemeris and clock biases, atmospheric delays, multipath, and receiver clock bias, as indicated in Equation (2). However, for short baseline applications such as those considered in this paper (<15 km), satellite ephemeris bias, satellite clock bias, receiver clock bias, and atmospheric delays can be assumed to have been eliminated through the use of the double-differencing (DD) algorithm. Thus, the main error source still remaining in the measurements is multipath, although in this paper it is assumed that such a multipath error can be modelled and/or mitigated in some way. In addition, if it is assumed that the DD ambiguities were successfully resolved before a certain epoch (and then eliminated from the model as an unknown), the ambiguity term in Equation (4) also disappears. As a consequence, Equation (2) can be rewritten:

$$\begin{aligned}\nabla\Delta\phi^{GPS} &= \phi_U^k - \phi_U^j - \phi_R^k + \phi_R^j \\ &= \frac{1}{\lambda}\nabla\Delta\rho_{UR}^{kj} + \nabla\Delta\varepsilon^{GPS}.\end{aligned} \tag{5}$$

The expected value of the measurement noise ($\nabla\Delta\varepsilon^{GPS}$) would be:

$$E\left[\nabla\Delta\varepsilon^{GPS}\right] = 0. \tag{6}$$

If two DD measurements are available, the covariance matrix is:

$$D\left[\nabla\Delta\varepsilon^{GPS}\right] = 2\sigma^2\begin{bmatrix}2 & 1\\ 1 & 2\end{bmatrix}. \tag{7}$$

https://doi.org/10.1017/S0373463303002443 Published online by Cambridge University Press

Hence, the variance of one DD measurement is $4 \cdot \sigma^2$ (Hofmann-Wellenhof *et al.*, 2001).

On the other hand, the errors ($\nabla\Delta\varepsilon^{INS}$) in the double-differenced geometric distances are mostly induced by the INS-predicted position errors. In order to analyse this error, both the receiver antenna position and satellite ephemeris biases have to be mapped into distance errors. The distance between a GPS satellite and user receiver (ρ_r^s) can be linearized with respect to their approximate values x_0^s, y_0^s, z_0^s and x_{r0}, y_{r0}, z_{r0}:

$$\rho_r^s = \rho_0 + \underbrace{\frac{x_{r0} - x_0^s}{\rho_0}}_{a_X}(\delta x_r - \delta x^s) + \underbrace{\frac{y_{r0} - y_0^s}{\rho_0}}_{a_Y}(\delta y_r - \delta y^s) + \underbrace{\frac{z_{r0} - z_0^s}{\rho_0}}_{a_Z}(\delta z_r - \delta z^s). \tag{8}$$

Assuming these initial coordinates are true values, the distance errors of the reference and mobile receivers caused by the satellite ephemeris and receiver position errors are:

$$\delta\rho_R^i = a_X^i(\delta x_R - \delta x^i) + a_Y^i(\delta y_R - \delta y^i) + a_Z^i(\delta z_R - \delta z^i). \tag{9}$$

$$\delta\rho_M^i = a_X^i(\delta x_M - \delta x^s) + a_Y^i(\delta y_M - \delta y^i) + a_Z^i(\delta z_M - \delta z^i). \tag{10}$$

If it is assumed that the satellite ephemeris errors are eliminated by double-differencing, the error ($\nabla\Delta\varepsilon^{INS}$) is:

$$\nabla\Delta\varepsilon^{INS} = \underbrace{(a_X^i - a_X^j)}_{A_X}\delta x_M + \underbrace{(a_Y^i - a_Y^j)}_{A_Y}\delta y_M + \underbrace{(a_Z^i - a_Z^j)}_{A_Z}\delta z_M. \tag{11}$$

If the expected values of the GPS/INS system's position error (X_{IP}) is zero with the assumption that the navigation parameters and sensor errors are reliably estimated (and corrected), and its covariance matrix can be obtained from the Kalman filter:

$$E(X_{\mathrm{IP}}) = 0, \quad P_{\mathrm{IP}} = \begin{bmatrix} \sigma_{xx} & \sigma_{xy} & \sigma_{xz} \\ \sigma_{yx} & \sigma_{yy} & \sigma_{yz} \\ \sigma_{xz} & \sigma_{yz} & \sigma_{zz} \end{bmatrix}, \tag{12}$$

then the expected values of ($\nabla\Delta\varepsilon^{INS}$) are zero as well if the remaining error sources are eliminated by double differencing. On the other hand the covariance matrix can be derived using the covariance propagation law:

$$D[\nabla\Delta\varepsilon^{INS}] = A P_{\mathrm{IP}} A^{\mathrm{T}}, \tag{13}$$

where,

$$A = \begin{bmatrix} A_X^{aj} & A_Y^{aj} & A_Z^{aj} \\ A_X^{bj} & A_Y^{bj} & A_Z^{bj} \\ \vdots & \vdots & \vdots \\ A_X^{ij} & A_Y^{ij} & A_Z^{ij} \end{bmatrix}. \tag{14}$$

Hence the decision values can be written as follows (keeping in mind the GPS error considerations mentioned above and the DD integer ambiguity is resolved in some

https://doi.org/10.1017/S0373463303002443 Published online by Cambridge University Press

previous epoch):

$$\delta\nabla\Delta\phi = \nabla\Delta\varepsilon^{GPS} + \nabla\Delta\varepsilon^{INS}. \tag{15}$$

Assume the GPS carrier phase measurements are uncorrelated in time, then the estimated position by INS and the actual carrier phase measurements are statistically uncorrelated since the estimated position is only affected by previous GPS measurements (Altmayer, 2000). Thus the expected values of the decision values are:

$$E[\delta\nabla\Delta\phi] = 0, \tag{16}$$

and the variance can be obtained as follows:

$$\sigma^2[\delta\nabla\Delta\phi] = \sigma^2[\nabla\Delta\varepsilon^{GPS}] + \sigma^2[\nabla\Delta\varepsilon^{INS}]. \tag{17}$$

As a consequence cycle slip detection and identification can be carried out through continuously performing a hypothesis test with respect to the decision values.

2.3. *Cumulative Sums (CUSUMS) Test.* The decision values ($\delta\nabla\Delta\phi$) represent the cycle slip indicating signals which makes possible not only the detection of slips but also permits their magnitude to be determined. Assuming that the signal is characterized by a Gaussian distribution with the static properties described in the preceding section (see Equations (16) & (17)), the CUSUM algorithm can be applied to detect the cycle slips.

Define the two statistical hypotheses H_0 and H_a. A sequence of $\delta\nabla\Delta\phi$ can be obtained, which is assumed to be a white noise process with constant mean value $\mu_i (i = 0, a)$:

$$\delta\nabla\Delta\phi = \begin{pmatrix} \mu_0 + e_t & \text{if } T \leqslant u-1 \\ \mu_a + e_t & \text{if } T \geqslant u \end{pmatrix}, \tag{18}$$

where, μ_0 is the mean value for the decision values before a cycle slip, μ_a is the mean value after the cycle slip and e_t is a white noise sequence with variance $\sigma^2[\delta\nabla\Delta\phi]$.

Given a sample of size T, denote the null hypothesis H_0 such that no change or departure from the initial conditions has taken place during the entire time sequence, while the alternative hypothesis H_a will be the one that corresponds to a slip occurring at the sampling position u. These hypotheses can therefore be expressed as:

$$\begin{pmatrix} H_0 : \mu = \mu_0 & \text{if } u \leqslant T \\ H_a : \mu = \mu_a & \text{if } u \leqslant T \end{pmatrix}. \tag{19}$$

The probability density functions of the decision values are:

$$f_i(x) = \begin{pmatrix} f(x|H_0) = \dfrac{1}{\sigma\sqrt{2\pi}} \exp\left(-\dfrac{(x-\mu_0)^2}{2\sigma^2} \right) & \text{if } H_0 \text{ is true} \\ f(x|H_a) = \dfrac{1}{\sigma\sqrt{2\pi}} \exp\left(-\dfrac{(x-\mu_a)^2}{2\sigma^2} \right) & \text{if } H_a \text{ is true} \end{pmatrix}, \tag{20}$$

where x represents the decision value $\delta\nabla\Delta\phi$. Since successive decision values are statistically independent, the logarithms of the likelihood of joint distribution density at the n-the sampling point can be written as a cumulative sum (CUSUM) (Mertikas

https://doi.org/10.1017/S0373463303002443 Published online by Cambridge University Press

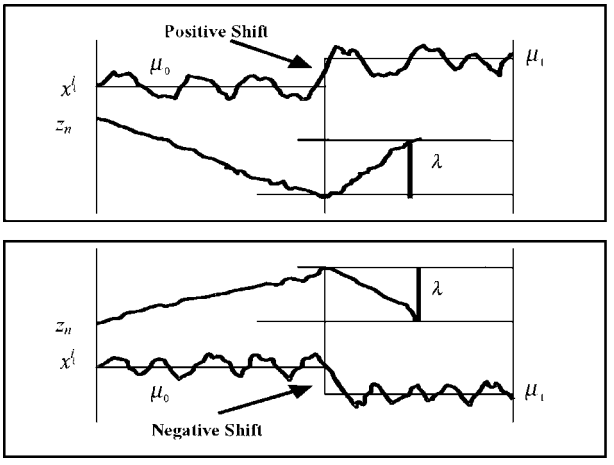

Figure 2. Typical behaviour of the CUSUM decision function.

& Rizos, 1997; Metikas, 2001):

$$s(n)=\ln\frac{f_a(x_1)}{f_0(x_1)}+\cdots+\ln\frac{f_a(x_n)}{f_0(x_n)}=z_1+z_2+\cdots+z_{n-1}+z_n, \tag{21}$$

where the single increment z_n can be derived from Equation (20):

$$\begin{aligned} z_n&=\ln f_a(x_n)-\ln f_0(x_n)=\frac{1}{2\sigma^2}\{(x_n-\mu_0)-(x_n-\mu_a)\}\\ &=\frac{\mu_a-\mu_0}{2\sigma^2}\left(x_n-\frac{\mu_a+\mu_0}{2}\right)=\frac{\delta\mu}{2\sigma^2}\left(x_n-\mu_0-\frac{\delta\mu}{2}\right). \end{aligned} \tag{22}$$

Generally speaking, the signal increment z_n is negative if the null hypothesis H_0 is true, whereas it is positive if the alternative hypothesis H_a is true in the case of positive shift, as indicated in Figure 2. Thus a shift in the mean value of the decision values (a cycle slip occurrence) is reflected as a change in the sign of the average value of the single increment of the log-likelihood ratio (Mertikas & Rizos, 1997; Metikas, 2001).

The CUSUM algorithms can be classified into two types. The first type is the one-sided CUSUM, which can be used when both the means before and after the change are known. The second type is the two-sided CUSUM, to be used when the change magnitude is unknown. It is the two-sided CUSUM test that should be used for the cycle slip detection algorithm with a minimum detectable jump ($\delta\mu_{\min}$). This test uses two CUSUM algorithms in parallel; the first one for detecting an increase in the mean, and the second for detecting a decrease in the mean of the sequence (Basseville, 1988; Basseville & Nikiforov, 1993; Hinkley, 1970). Thus, a slip will be detected if:

$$\begin{cases} g_n^*=s_n^*-\min\limits_{0\leqslant t\leqslant n} s_t^*\geqslant\lambda^*\\ g_n^*=\max\limits_{0\leqslant t\leqslant n} s_t^*-s_n^*\geqslant\lambda^*, \end{cases} \tag{23}$$

https://doi.org/10.1017/S0373463303002443 Published online by Cambridge University Press

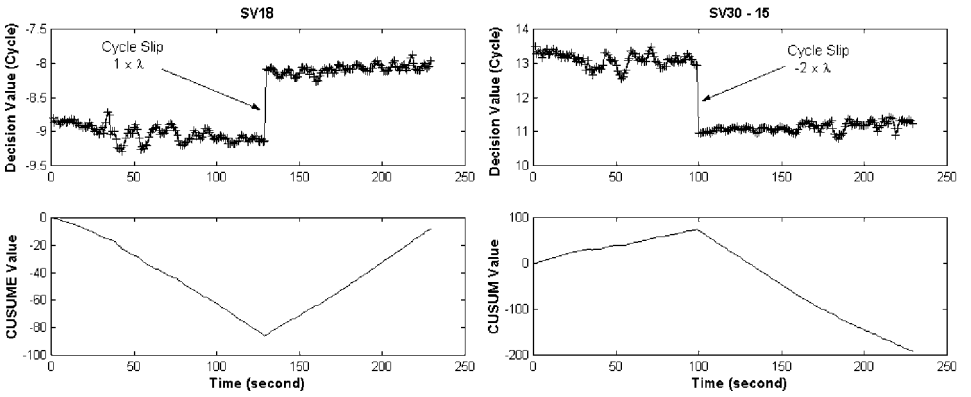

Figure 3. The cumulative sums for detecting one cycle slip in L1 carrier phase measurement.

where,

$$s_t^* = s_{t-1}^* + \frac{\delta\mu_{\min}}{2\sigma^2}\left(x_t - \mu_0 - \frac{\delta\mu_{\min}}{2}\right),\ s_0^* = s_0^* = 0. \tag{24}$$

To avoid the downward drift of the CUSUM across and out of the page limits, an algebraic equivalent of Equation (23) is used (Hawkins and Olwell, 1998; Mertikas, 2001):

$$\begin{cases} C_n^* = \max(0,\ C_{n-1}^* + g_n^*) \geqslant \lambda^* \\ C_n^* = \min(0,\ C_{n-1}^* + g_n^*) \geqslant \lambda^* \end{cases},\ C_n^* = C_n^* = 0. \tag{25}$$

The resulting alarm time is given by:

$$t_a = \min\{t \geqslant 1:\ (g_t^* \geqslant \lambda) \cup (g_t^* \geqslant \lambda)\}. \tag{26}$$

In most cases very little is known about the change magnitude $\delta\mu_{\min}$. Three possible *a priori* choices can be made with respect to this parameter. The first is to choose $\delta\mu_{\min}$ as a minimum possible jump magnitude (limit case being $\delta\mu_{\min} = 0$). The second is to choose *a priori* the most likely jump magnitude. The third choice is a worst-case value from the point of view of the cost of missed detection(s). If the actual change in mean is less than that specified in the CUSUM test, then the single increments z_n of the log-likelihood ratio will always have a positive mean and the CUSUM scheme will be ineffective as a detector of change. It is common to specify a rejectable level $\delta\mu_{\min}$, then determine the threshold value λ so that the CUSUM test has a specified maximum rate of detection alarm with a minimum delay. A more detailed description of CUSUM parameter tuning is given in Hawkins & Olwell (1998) and Mertikas & Rizos (1997).

Figure 3 shows examples of the cumulative sum tests for detecting cycle slips. The upper graphs depict the calculated decision values, whereas the lower graphs show the CUSUM values computed from Equation (23). Cycle slips were simulated in L1 carrier phase measurements, namely $+1$ cycle on PRN15 and -2 cycles on PRN30. A cycle slip at the $n = 130$, 100 sampling step is reflected as a change of the positive and negative trend in the cumulative sum. The onset time could be reliably determined as the last time a minimum value of the log-likelihood occurred.

https://doi.org/10.1017/S0373463303002443 Published online by Cambridge University Press

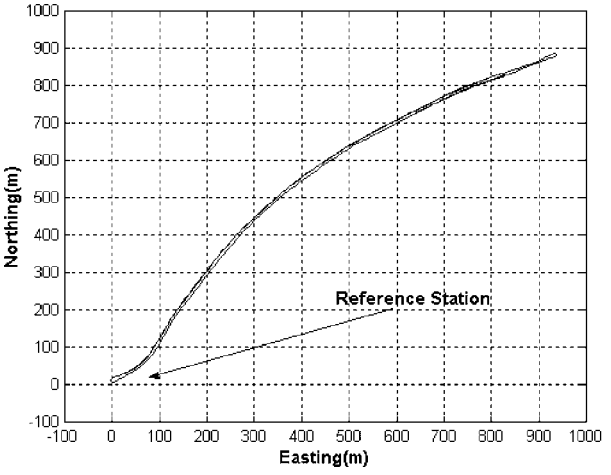

Figure 4. A vehicle trajectory during the data acquisition.

3. FIELD TESTS AND RESULTS.

3.1. *General Description of the Test*. To illustrate the effectiveness of the proposed algorithm to detect and correct cycle slips, kinematic experiments were carried out on Prince of Wales Road in Sydney, on the 21th October 2002. The IMU used in this research was the Boeing C-MIGITS II, which is considered to be a tactical-level accuracy unit (5 deg/h, 500 μg), compact (8 cm × 9 cm × 12 cm), and lightweight (1·1 kg). The IMU outputs delta angle and delta velocity measurements for navigation solutions at a rate of 100 Hz, as well as acceleration and angular velocity for flight control or sensor stabilization at 600 Hz. In addition, two NovAtel OEM3 Millennium GPS receivers were used in both the reference and rover (vehicle) stations. The GPS antenna and IMU was mounted on the roof of the test vehicle. Raw IMU measurements were recorded at 100 Hz, while dual-frequency GPS data were logged at 1 Hz. Both GPS and IMU data were logged through a single serial port on two laptop computers. At the same time, RTK (Real Time Kinematic) processed results were recorded to evaluate the position accuracy of the integrated GPS/INS system. During the experiment there were 6 visible satellites (above the cut-off angle of 15°). As shown in Figure 4 (vehicle trajectory), the separation between reference and mobile receivers reaches up to 1 km.

3.2. *Algorithm's Performance*. The raw IMU and GPS data from the NovAtel OEM3 Millennium were processed using in-house software package – a modified version of the AIMS^{TM} navigation processing software (Lee *et al.*, 2002). While the software was originally designed for Trimble 4000ssi GPS receivers and the Litton LN-100 INS, it has been modified to accept C-MIGITS II data. For this study, further modifications have been made to include the cycle slip detection and correction algorithm described earlier. In addition, it should be noted that only L1 measurements were used for the Kalman filter update in this study.

First of all, CUSUM parameters were set, 0·3 and 0·5 cycle (approximate 9 cm) for the threshold (λ) and the minimum detectable value ($\delta\mu_{\min}$) respectively. Since it is

https://doi.org/10.1017/S0373463303002443 Published online by Cambridge University Press

Table 1. Simulated L1 cycle slips.

PRN number	Simulated CS Period (GPS second)	Simulated CS Magnitude
18	96434–96934	+1
	96484	+1
	96534–96934	−2
	96584	−2
	96434–96934	+1
	96484	+2
23	96534–96934	+10
	96784–96934	−20
	96684–96934	+10
26	96484	+1
	96584	−2
	96884	+2

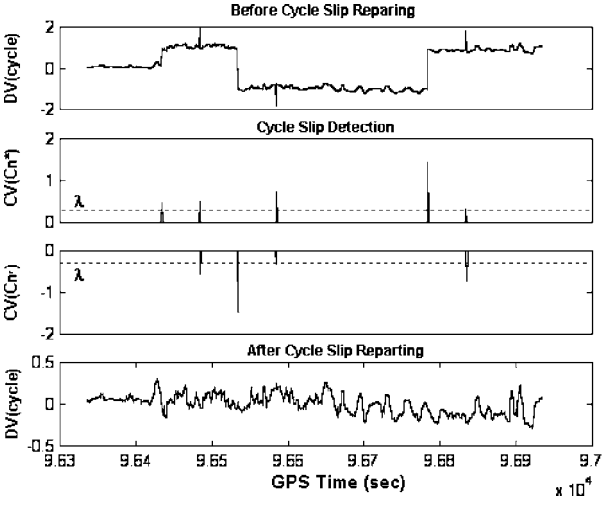

Figure 5. CUSUM test for PRN 18.

difficult to evaluate the algorithm's performance without knowing the truth, the cycle slips were simulated. The slips can be simulated by adding an integer number of wavelengths to the raw L1 carrier phase observables. The simulated cycle slip scenario is shown in Table 1. All cycle slips were only inserted into the observables for the mobile receiver.

Figures 5–7 show the decision values *before*/*after* the correction and the two-sided CUSUM values of PRN18, 23, and 26 (with reference PRN27). It is important to emphasize that the CUSUM values were computed using Equation (26) instead of Equation (24) to avoid the upward or downward drift of the CUSUM values across and out of the page limits. The first graphs in those figures depict the decision values ($\delta\nabla\Delta\phi$) with the cycle slips imposed in the raw measurements. The second and third graphs show the CUSUM values (C_n^*, C_n^*). It can be seen from those figures that the values are zero when no cycle slip is present. This actually stems from the fact that

https://doi.org/10.1017/S0373463303002443 Published online by Cambridge University Press

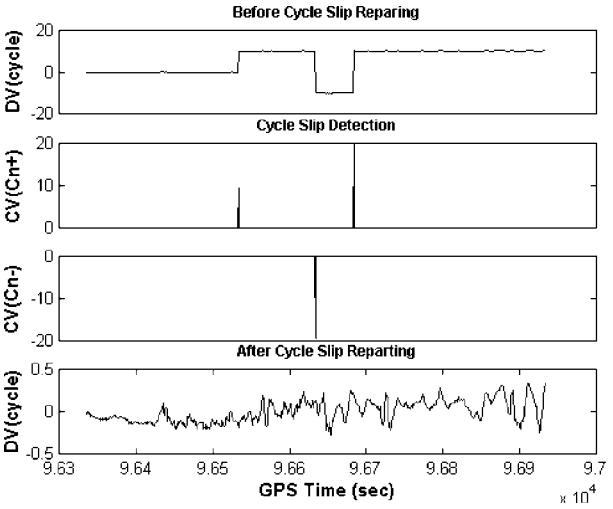

Figure 6. CUSUM test for PRN 23.

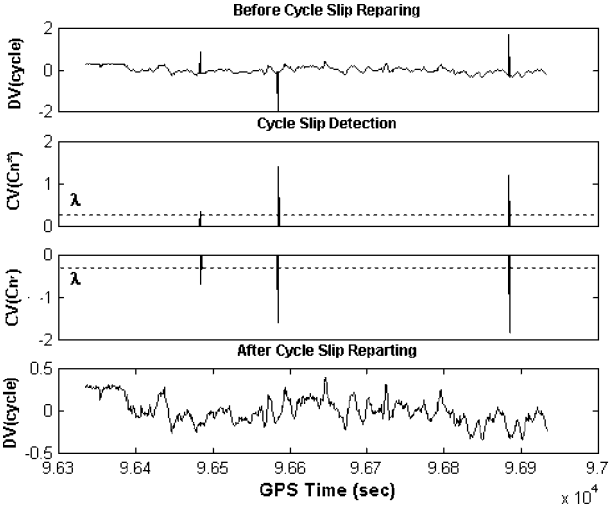

Figure 7. CUSUM test for PRN 26.

there is no abrupt change in the decision values except for the cycle slips. It means that small peaks do appear in the CUSUM value graph if there are larger errors in the INS navigation computation. As a whole, it is expected that their magnitude is smaller than the threshold (λ). It must be emphasized that the minimum detectable value ($\delta\mu_{\min}$) and the threshold (λ) have to be very carefully selected. When the cycle slip occurs, the detection threshold is exceeded. The third graphs illustrate the decision values after cycle slip correction. It is obvious from those figures that the algorithm performs very well, the slipped carrier phase measurements are precisely detected and successfully corrected even if the slips are only one cycle.

Figure 8 shows the navigation parameters and RMS values for Kalman-filtering obtained by an integrated GPS/INS system. The first graph in the left column depicts the system positioning accuracy compared with GPS antenna position provided by

https://doi.org/10.1017/S0373463303002443 Published online by Cambridge University Press

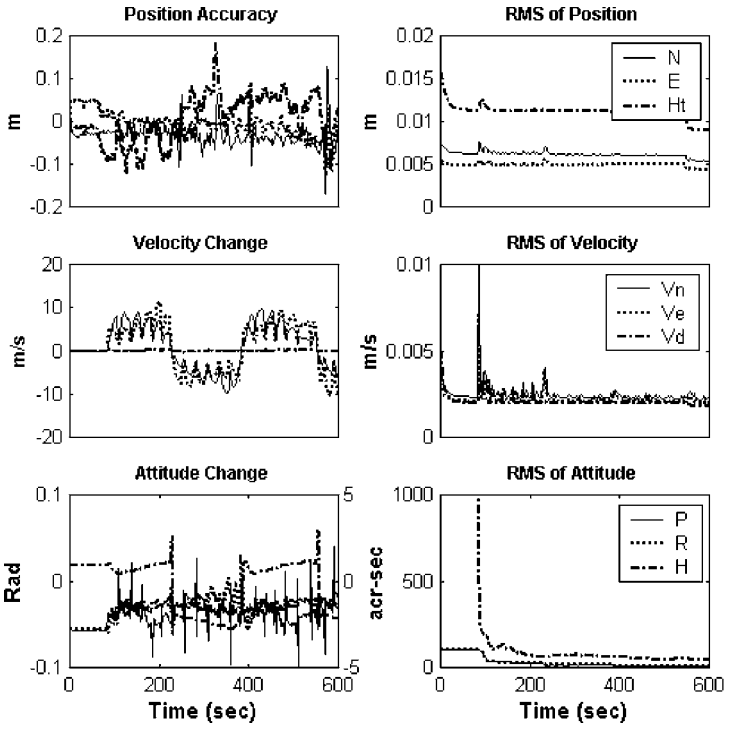

Figure 8. Navigational parameters and RMSs of Kalman filtering.

RTK positioning, which typically provides an accuracy of a few centimetres as long as the carrier phase ambiguities are resolved correctly. The second and third graphs in the same column show velocity and attitude changes. However, the right column shows RMS values of the estimated navigation parameters. It is very important to note that all the results in the figure indicate that the integration system accuracy and performance can be maintained when the cycle slip detection and identification algorithm proposed in this paper is implemented.

4. CONCLUDING REMARKS. Cycle slips are the biggest GPS error source if they remain in the raw carrier phase measurements, in that they are mainly absorbed by the integer ambiguities and hence lead to biased estimates for the navigation parameters in GPS-based navigation systems. Therefore it is crucial to detect and correct cycle slips. In this paper a cycle slip detection and identification scheme was developed for use with integrated GPS/INS systems. The algorithm uses additional GPS antenna positions provided by the INS navigation solutions, and the cumulative-sum (CUSUM) test is applied in order to detect the slips. Hence it can be easily implemented within the system integration software. The results of field tests indicate that cycle slips can be effectively detected and subsequently corrected using the proposed algorithm. Further research will be conducted in order to extend the applicability of the algorithm to high multipath environments and for long baselines.

https://doi.org/10.1017/S0373463303002443 Published online by Cambridge University Press

ACKNOWLEDGEMENTS

Lee H.K. is supported in his PhD research by a scholarship funded by the Kwanjeong Educational Foundation of Korea.

REFERENCES

Altmayer, C. (2000). Enhancing the integrity of integrated GPS/INS system by cycle slip detection and correction, *Proceedings of the IEEE intelligent Vehicles Symposium*, Dearborn, Miami, October 3–5, 174–179.

Bassevile, M. (1988). Detecting changes in signals and systems – a survey, *Automatica*, **24**(3), 309–326.

Basseville, M. & V. Nikiforov (1993). *Detection of Abrupt Changes – Theory and Applications*, Prentice Hall, New Jersey, 441pp.

Blewitt, G. (1990). An automatic editing algorithm for GPS data, *Geophysical Research Letters*, **17**(3), 199–202.

Cannon, M. E. (1987). *Kinematic Positioning Using GPS Pseudoranges and Carrier Phase Observations*, UCGE Report No. 20019, Department of Geomatics Engineering, The University of Calgary, Alberta, Canada.

Dedes, G. & A. Mallett (1995). Effects of the ionosphere and cycle-slips in long baseline dynamic positioning, *Proceedings of Mobile Mapping Symposium*, Columbus, Ohio, May 24–26. 142–152.

Gao, Y. (1992). *A Robust Quality Control System for GPS Navigation and Kinematic Positioning*, UCGE Report No. 20075, Department of Geomatics Engineering, The University of Calgary, Alberta, Canada, 152pp.

Gao, Y. & Z. Li (1999). Cycle slip detection and ambiguity resolution algorithms for dual-frequency GPS data processing, *Marine Geodesy*, **22**(4), 161–181.

Han, S. (1997). *Carrier Phase-Based Long-Range GPS Kinematic Positioning*, UNISURV S-49, PhD Thesis, School of Surveying and Spatial Information Systems, The University of New South Wales, Sydney, Australia, 185pp.

Hawkins, M. D. & D. H. Olwell (1998). *Cumulative Sum Charts and Charting for Quality Improvement* (Statistics for engineering and physical science), Berlin/Heidelberg: Springer Verlag, 247pp.

Hinkley, D. (1970). Inference about the change point in a sequence of random variables, *Biometrika*, **57**(1), 1–17.

Hofmann-Wellenhof, B., H. Lichtenegger & J. Collins (2001). *GPS Theory and Practice*, 5th Edition, Springer-Verlag, Wien, 382pp.

Lee, H. K., J. Wang, C. Rizos & D. Grejner-Brzezinska (2002). GPS/Pseudlite/INS integration: Concept and first tests, *GPS Solutions*, **6**(1–2), 34–46.

Mertikas, S. P. (2001). Automatic and on-line detection of small but persistent shifts in GPS station coordinates and statistical process control, *GPS Solutions*, **5**(1), 39–50.

Mertikas, S. P. & C. Rizos (1997). Online detection of abrupt changes in the carrier phase measurements of GPS, *Journal of Geodesy*, **71**, 469–482.

Ogaja, C. (2002). *A Framework in Support of Structural Monitoring by RTK-GPS and Multisensor Data*, PhD Thesis, School of Surveying and Spatial Information Systems, The University of New South Wales, Sydney, Australia, 207pp.

Rizos, C. (1999). Quality issues in real-time GPS positioning, Final Report of the IAG SSG 1.154, (Available on-line at: http://www.gmat.unsw.edu.au/ssg_RTQC/ssg_rtqc.pdf).

Schwarz, K. P., N. El-Sheimy & Z. Liu (1994). Fixing GPS cycle slips by INS/GPS – Method and experience, *Proceedings of International Symposium on Kinematic Systems in Geodesy, Geomatics and Navigation*, Banff, Canada, August 30–September 2, 265–275.

Wei, M., M. E. Cannon & K. P. Schwarz (1992). Maintaining high accuracy GPS positioning 'on the fly', *Proceedings of IEEE Position Location and Navigation Symposium*, March 23–27, 403–411.